Distorted *bcc* Indium Cubes as Structural Motifs in Ca[TIn_4] (T = Rh, Pd, Ir)

Rolf-Dieter Hoffmann and Rainer Pöttgen*[a]

Abstract: The title compounds were prepared from the elements by reactions in water-cooled glassy carbon crucibles under an argon atmosphere in a high-frequency furnace. $CaPdIn_4$ crystallizes with the $YNiAl_4$-type structure: *Cmcm*, $a = 446.7(3)$, $b = 1665(1)$, $c = 754.3(5)$ pm, $wR2 = 0.0465$ with 646 F^2 values and 24 variables. The structure is built up from a complex three-dimensional [$PdIn_4$] polyanion in which the calcium atoms occupy distorted pentagonal tubes formed by indium and palladium atoms. $CaRhIn_4$ and $CaIrIn_4$ adopt the $LaCoAl_4$-type structure: *Pmma*, $a = 867.6(1)$, $b = 422.91(8)$, $c = 745.2(1)$ pm, $wR2 = 0.0583$ with 468 F^2 values and 24 variables for $CaRhIn_4$; $a = 869.5(1)$, $b = 424.11(6)$, $c = 746.4(1)$ pm, $wR2 = 0.0614$ 471 F^2 values with 24 variables for $CaIrIn_4$. This structure type, too, has a three-dimensional [$RhIn_4$] polyanion which is related to the structure of binary $RhIn_3$. The calcium atoms fill distorted pentagonal prismatic channels formed by indium atoms. Semi-empirical band structure calculations for $CaRhIn_4$ and $CaPdIn_4$ reveal strongly bonding In–In, Rh–In and Pd–In interactions but weaker Ca–Rh, Ca–Pd and Ca–In interactions. $CaRhIn_4$ and $CaPdIn_4$ are compared with other indium-rich compounds such as $YCoIn_5$ and Y_2CoIn_8, and with elemental indium. Common structural motifs of the indium-rich compounds are distorted *bcc*-like indium cubes.

Keywords: calcium · chemical bonding · electronic structure · indium · structure elucidation

Introduction

Ternary alkaline earth (AE) – transition metal (T) – indium systems include a variety of interesting compounds with peculiar crystal structures. In the past the main focus of investigation was the ternary system Ca–T–In with copper or nickel as the transition metal component. Several compounds were reported, covering a wide range of compositions: $CaCu_{9-x}In_{2+x}$, $CaCu_{6.5}In_{5.5}$, $CaCu_{4+x}In_{1-x}$, $CaCu_{0.5}In_{1.5}$, $CaCuIn_2$, $CaNiIn_2$ and $CaNiIn_4$.[1–3]

The degree of In–In bonding in these intermetallics seems to depend strongly on the indium content as well as on the electron count. In equiatomic TiNiSi-type CaAuIn[4] the indium atoms are separated from each other by 349 pm; thus, no In–In bonding is observed within the three-dimensional [AuIn] polyanion, which is composed of distorted $InAu_{4/4}$ tetrahedra. In isotypic SrPtIn[5] and EuRhIn[6] In–In bonding becomes more important, with In–In distances of 335 pm (SrPtIn) and 325 pm (EuRhIn), clearly indicating that electrons from In–In bonding states are taken by the more electron-poor transition metals to fill their d states, which in turn lowers the occupancy of antibonding indium states, thus leading to shorter In–In distances.

[a] Priv.-Doz. Dr. R. Pöttgen, Dr. R.-D. Hoffmann
Anorganisch-Chemisches Institut, Universität Münster
Wilhelm-Klemm-Straße 8, 48149 Münster (Germany)
E-mail: pottgen@uni-muenster.de

A higher degree of In–In bonding has already been observed in $Sr_2Rh_2In_3$,[7] with just a slightly higher indium content. In the two-dimensional [Rh_2In_3] polyanion there are two different indium sites: one has two indium neighbours in the coordination sphere, each at a distance of 318 pm; the other has three close indium neighbours, two at In–In distances of 303 pm and one at 318 pm, whereas its fourth indium neighbour, completing the distorted tetrahedral indium environment at 361 pm, has no bonding interaction.

Orthorhombically distorted tetrahedral networks of indium also occur in the compounds $CaTIn_2$ (T = Ni, Cu, Rh, Pd, Ir, Pt, Au)[1–3, 8, 9] and $SrTIn_2$ (T = Rh, Pd, Ir, Pt).[10] They crystallize in two structural types. $CaIrIn_2$ is of the $CaRhIn_2$ type, whereas the other compounds are isotypic with $MgCuAl_2$. The indium networks are derived from the well-known structure of hexagonal diamond (lonsdaleite[11]). The structures of $CaTIn_2$ and $SrTIn_2$ are best described as filled variants of the well-known Zintl phases $CaIn_2$ and $SrIn_2$.[12] The modulation of the In–In distances again clearly depends on the electron count.

The distorted tetrahedral indium networks collapse if the indium content is further increased, as in $EuNiIn_4$,[13] $EuCuIn_4$,[1, 14] $YCoIn_5$[15] and Y_2CoIn_8.[15] Here *bcc*-like indium cubes similar to those in elemental indium occur,[11] but in the known ternary compounds In–In distances are generally shorter than in elemental indium. The same holds true for binary indium compounds such as TIn_3 (T = Co, Ru, Rh, Ir).[16, 17]

0947-6539/00/0604-0600 $ 17.50+.50/0 *Chem. Eur. J.* **2000**, *6*, No. 4

We extended our research on In–In bonding to indium-rich compounds containing alkaline earth and late transition metals. Here we report on the synthesis and chemical bonding of the new indium-rich compounds $CaTIn_4$ (T = Rh, Pd, Ir). Excerpts of this work have been presented recently at a conference.[7]

Experimental Section

Synthesis: Starting materials for the preparation of $CaTIn_4$ (T = Rh, Pd, Ir) were calcium granules (Johnson Matthey; 99.5%, redistilled), rhodium, palladium and iridium powder (Degussa; 200-mesh, >99.9%) and indium teardrops (Johnson Matthey; >99.9%). The large alkaline earth metal ingots were cut into small pieces, then kept in Schlenk tubes under argon before reaction.

$CaPdIn_4$ and $CaRhIn_4$ were prepared by high-frequency melting (Hüttinger Elektronik, Freiburg; type TIG 1.5/300) of the elements in glassy carbon crucibles (Sigradur® G, glassy carbon, type GAZ006) under flowing argon. For $CaRhIn_4$ the ideal ratio of the constituent elements was employed, but for the synthesis of $CaPdIn_4$ several mixtures with Ca:Pd:In ranging from 1:1:4 to 1:1:10 were made to react (see below). The argon was purified over silica gel, molecular sieves and titanium sponge (900 K). The glassy carbon crucibles were placed in a water-cooled Duran® glass sample chamber. The experimental set-up is described in detail elsewhere.[4] During the inductive heating process, the final reaction of the calcium granules with the alloy formed initially from the noble metals and indium at low temperature is strongly exothermic. To ensure homogeneity and good crystallization the samples were held for about another hour at 800–900 K. No weight losses were observed for these reactions. After being cooled to room temperature, the samples could easily be separated from the glassy carbon crucibles by tapping their bases. No reaction of the samples with the crucibles could be detected.

An alternative two-step synthesis route was preferred for the preparation of $CaIrIn_4$. Since the melting point of iridium is high (2680 K) compared with those of calcium (1120 K) and indium (430 K), the reactions often led to inhomogeneous products, as already described for $EuIrSn_2$[6] and $CaIrIn_2$.[9] Use of a precursor, however, lessens the force of the exothermic reaction between calcium and the initially formed iridium–indium alloy. Thus, $CaIrIn_2$ was prepared as described above and used as a precursor for the next step. A prereacted sample with nominal composition $CaIrIn_2$ was coarsely ground and remelted with the required amount of elemental indium in a glassy carbon crucible. To increase the crystallinity the sample was kept for about an hour at approximately 800 K and cooled to room temperature. The brittle product contained about 90% $CaIrIn_4$ agglomerated with $IrIn_3$.

Scanning electron microscopy: Various samples of $CaTIn_4$ (T = Rh, Pd, Ir) were investigated in more detail by metallography. The microstructures of polished ingots of these indium compounds were left unetched and analysed with a Leica 420I scanning electron microscope in the back-scattering mode. The EDX (energy dispersive analysis of X-rays) measurements were carried out on mounted single crystals, untreated fragments and polished samples. Wollastite, InAs, Rh, Pd and Ir were used as internal standards.

X-ray investigations: Guinier powder patterns of each sample were recorded with $Cu_{K\alpha_1}$ radiation with α-quartz ($a = 491.30$, $c = 540.46$ pm) as an internal standard. To ensure correct indexing of the diffraction lines, the observed patterns were compared with calculated ones[18] by using the positional parameters of the refined structures. The lattice constants were obtained by least-squares refinements of the Guinier powder data. Single-crystal intensity data were collected at room temperature by use of a four-circle diffractometer (Enraf–Nonius CAD4) with graphite monochromatized $Mo_{K\alpha}$ radiation ($\lambda = 71.073$ pm) and a scintillation counter with pulse height discrimination. Scans were taken in the $\omega/2\theta$ mode. Empirical absorption corrections were applied on the basis of ψ-scan data. All other relevant crystallographic data and details concerning the data collections are listed in Table 1.

Band structure calculations: Three-dimensional semi-empirical band structure calculations were based on an extended Hückel Hamiltonian,[19, 20] whereas off-site Hamiltonian matrix elements were evaluated according to the weighted Wolfsberg–Helmholtz formula,[21] minimizing counterintuitive orbital mixing. The minimal orbital basis set was composed of Slater orbitals that had been scaled to *j*-averaged values of numerical Dirac–Fock atomic functions; on-site Hamiltonian matrix elements were approximated by averaged atomic orbital energies from the same source.[22, 23] For greater accuracy, the Rh 4d, Pd 4d and Ir 5d atomic wavefunctions were approximated by double-ξ functions. The exchange integrals, ξ orbital exponents and weighting coefficients are listed in Table 2. The eigenvalue problem was solved in reciprocal space at 112 ($CaRhIn_4$, $CaIrIn_4$) and 120 ($CaPdIn_4$) points within the irreducible wedge of the Brillouin zone with the Yaehmop code.[24]

Abstract in German: *Die Titelverbindungen wurden aus den Elementen durch Reaktion in wassergekühlten Glaskohlenstofftiegeln unter Argonatmosphäre in einem Hochfrequenzofen synthetisiert. $CaPdIn_4$ kristallisiert mit der $YNiAl_4$ Struktur: Cmcm, a = 446,7(3), b = 1665(1), c = 754,3(5) pm, wR2 = 0.0465 646 F^2 Werte und 24 Variable. Die Struktur besteht aus einem komplexen dreidimensionalen $[PdIn_4]$ Polyanion, in dem die Calciumatome verzerrte, pentagonale Kanäle, die aus Indium- und Palladiumatomen gebildet werden, besetzen. $CaRhIn_4$ und $CaIrIn_4$ haben die $LaCoAl_4$ Struktur: Pmma, a = 867,6(1), b = 422,91(8), c = 745,2(1) pm, wR2 = 0.0583 468 F^2 Werte für $CaRhIn_4$ und a = 869,5(1), b = 424,11(6), c = 746,4(1) pm, wR2 = 0.0614 471 F^2 Werte für $CaIrIn_4$, mit je 24 Variablen. Auch dieser Strukturtyp hat ein dreidimensionales $[RhIn_4]$ Polyanion, welches demjenigen in binärem $RhIn_3$ ähnelt. Die Calciumatome besetzen aus Indiumatomen gebildete pentagonal-prismatische Kanäle. Semi-empirische Bandstrukturrechnungen an $CaRhIn_4$, $CaIrIn_4$ und $CaPdIn_4$ ergeben stark bindende In–In, Rh–In, Ir–In und Pd–In Wechselwirkungen im Gegensatz zu schwächeren Ca–Rh, Ca–Ir, Ca–Pd und Ca–In Wechselwirkungen. $CaRhIn_4$ und $CaPdIn_4$ werden mit anderen indiumreichen Verbindungen wie $YCoIn_5$ und Y_2CoIn_8 sowie mit elementarem Indium verglichen. Gemeinsame Strukturmerkmale der indiumreichen Verbindungen sind verzerrte bcc ähnliche Indium-Würfel.*

Results and Discussion

Polycrystalline samples of $CaTIn_4$ (T = Rh, Pd, Ir) are light grey and stable in air over long periods of time. No decomposition was observed after several months. Single crystals have a very irregular platelet-like shape and exhibit a metallic lustre. Large single crystals of $CaPdIn_4$ can be plastically deformed. The EDX analyses revealed compositions close to the ideal atomic ratio of Ca:(Rh, Pd, Ir):In = 16.6:16.6:66.7. Average values [atom%] were 16:16:68 ($CaRhIn_4$), 16:18:66 ($CaPdIn_4$) and 18:16:66 ($CaIrIn_4$).

Metallography: Microstructure analyses of $CaRhIn_4$ and $CaPdIn_4$ gave very instructive information on the crystallization processes involved. For $CaRhIn_4$ primary crystallization can be assumed. Large grains of $CaRhIn_4$ show only small amounts of inclusions consisting of a core of RhIn surrounded by secondary peritectic $RhIn_3$ (Figure 1, top). These inclusions are the first reaction products at low temperature (at about the melting point of indium, 430 K), when an alloy is formed

Table 1. Crystal data and structure refinements for $CaRhIn_4$, $CaPdIn_4$ and $CaIrIn_4$.

	$CaRhIn_4$	$CaPdIn_4$	$CaIrIn_4$
M_w	602.27	605.76	691.56
crystal system	orthorhombic	orthorhombic	orthorhombic
space group	*Pmma* (No. 51)	*Cmcm* (No. 63)	*Pmma* (No. 51)
Pearson symbol	oP12	oC24	oP12
a [pm]	867.6(1)	446.7(3)	869.5(1)
b [pm]	422.91(8)	1665(1)	424.11(6)
c [pm]	745.2(1)	754.3(5)	746.4(1)
V [nm^3]	0.2734(1)	0.5610(2)	0.2753(1)
Z	2	4	2
ρ_{calcd} [g cm^{-1}]	7.32	7.17	8.34
crystal size [μm^3]	$20 \times 20 \times 50$	$15 \times 30 \times 35$	$10 \times 25 \times 35$
transmission (max:min)	1.15	1.87	2.28
μ [mm^{-1}]	20.3	20.1	41.4
F (000)	522	1048	586
θ range for data collection	2–30°	2-35°	2–30°
index range hkl	$\pm 12, +5, \pm 10$	$\pm 6, \pm 25, \pm 10$	$\pm 12, +5, \pm 10$
total no. reflections	1699	3768	1711
independent reflections	468 ($R_{int} = 0.0306$)	646 ($R_{int} = 0.0381$)	471 ($R_{int} = 0.0723$)
reflections with $I > 2\sigma(I)$	428 ($R_{sigma} = 0.0227$)	534 ($R_{sigma} = 0.0222$)	341 ($R_{sigma} = 0.0550$)
data/restraints/parameters	468/0/24	646/0/24	471/0/24
goodness-of-fit on F^2	1.200	1.105	1.101
final R indices [$I > 2\sigma(I)$]	$R1 = 0.0245$	$R1 = 0.0174$	$R1 = 0.0254$
	$wR2 = 0.0555$	$wR2 = 0.0401$	$wR2 = 0.0491$
R indices (all data)	$R1 = 0.0282$	$R1 = 0.0300$	$R1 = 0.0624$
	$wR2 = 0.0583$	$wR2 = 0.0465$	$wR2 = 0.0614$
extinction coefficient	0.060(2)	0.0011(1)	0.0035(3)
largest diff. peak/hole [e Å^{-3}]	1.36/ – 2.88	1.63/ – 1.78	4.03/ – 2.89

Table 2. Extended Hückel parameters.

Atom	Orbital	H_{ii} [eV]	ξ_1	c_1	ξ_2	c_2
Ca	4s	– 5.342	1.069			
	4p	– 3.569	0.893			
Rh	5s	– 6.208	1.617			
	5p	– 3.253	1.160			
	4d	– 11.600	3.577	0.794	1.542	0.343
Pd	5s	– 9.224	1.658			
	5p	– 3.279	1.182			
	4d	– 8.985	3.746	0.815	1.501	0.338
In	5s	– 10.790	2.020			
	5p	– 5.350	1.470			
Ir	6s	– 8.146	1.933			
	6p	– 4.171	1.308			
	5d	– 12.866	3.968	0.780	1.813	0.371

which then reacts at higher temperature with the calcium granules. These inclusions can no longer participate in the reaction equilibrium, because the surrounding ternary $CaRhIn_4$ matrix prevents further reaction with calcium or with the $CaIn_2$ that is probably formed. However, "$CaIn_2$" was dissolved during the polishing procedure, so that only traces of unknown hydrolysis products could be found at a very few grain boundaries.

The situation was quite different for $CaPdIn_4$. Metallographic investigations indicate that $CaPdIn_4$ forms peritectically from the melt and is in equilibrium with elemental indium, at least at high temperature. No indication of further Ca–Pd–In compounds with a higher indium content was found. A sample with the ideal atomic ratio of 1:1:4 clearly showed primary crystallization of $CaPdIn_2$ with $CaPdIn_4$ at the grain boundaries, and a surrounding eutectic phase consisting of $CaPdIn_4$ and elemental indium (Figure 1, bottom). Primary $CaPdIn_2$ is enveloped by more darkly

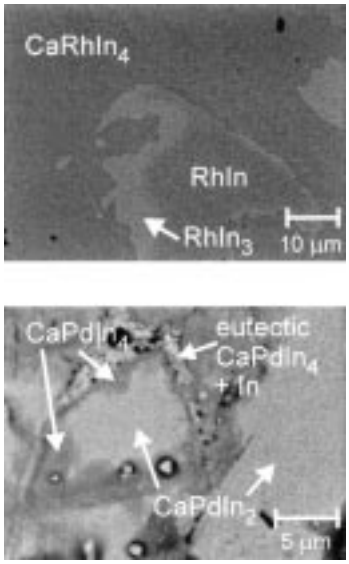

Figure 1. Scanning electron micrographs (backscattering mode) of polished unetched samples with nominal composition Ca:(Rh, Pd):In = 1:1:4, illustrating the crystallization behaviour of $CaRhIn_4$ (top) and $CaPdIn_4$ (bottom). The mid-grey RhIn core is enveloped by light grey peritectic $RhIn_3$ in a matrix of grey primary $CaRhIn_4$. In contrast, $CaPdIn_4$ is formed peritectically. A small envelope of grey $CaPdIn_4$ surrounds the light grey primary $CaPdIn_2$ core. The eutectic phase between the grains consists of very small particles of elemental indium and $CaPdIn_4$ with diameters of about 50 nm and less.

coloured, peritectic $CaPdIn_4$; thus, a peritectic reaction, $CaPdIn_2 + In_{liq} \Leftrightarrow CaPdIn_4$, was evident. Similar behaviour was observed previously for $CaAuIn_2$, which was found to be formed by the reaction $CaAuIn + In_{liq} \Leftrightarrow CaAuIn_2$.[8] Additional annealing of the sample with initial composition Ca:Pd:In = 1:1:4 was not promising, because it was not

0947-6539/00/0604-0602 $ 17.50+.50/0 *Chem. Eur. J.* **2000**, *6*, No. 4

possible to grind the ductile sample for a subsequent homogenizing step at low temperature. For the crystallization of $CaPdIn_4$, samples with a higher indium content (Ca:Pd:In = 1:1:4.5, 1:1:6 and 1:1:10) were therefore prepared. The sample with Ca:Pd:In = 1:1:6 still contained cord $CaPdIn_2$ with an envelopment of $CaPdIn_4$ next to small grains of primary $CaPdIn_4$. The 1:1:10 sample, however, contained platelet-like single crystals composed exclusively of primary $CaPdIn_4$ as large as 1 mm long and about 0.1 mm thick, separated by a ductile eutectic ($CaPdIn_4$ and elemental indium). Moreover, the single crystals could be extracted from the porous sample, because the excess indium was on top of a bundle of agglomerated crystals of $CaPdIn_4$. Unfortunately, the separated single crystals were not suitable for physical property measurements because of the adherent eutectic.

Lattice constants: The structural similarity of $CaPdIn_4$ to the $YNiAl_4$-type structure[25] was instantly visible on the Guinier film. The powder pattern could be indexed with a *C*-centred orthorhombic cell with the lattice constants listed in Table 1. The $CaRhIn_4$ and $CaIrIn_4$ patterns showed primitive orthorhombic lattices and the systematic extinctions were compatible with space group *Pmma*.

Structure refinements: Single crystals of $CaPdIn_4$, $CaRhIn_4$ and $CaIrIn_4$ were isolated from the annealed samples by mechanical fragmentation and examined by Buerger precession photographs to establish both symmetry and suitability for intensity data collection.

The photographs of $CaRhIn_4$ (reciprocal layers $hk0$, $hk1$ and $0kl$) and of $CaIrIn_4$ ($h0l$) showed orthorhombic Laue symmetry *mmm* and the only systematic extinctions found were those for an *a* glide plane perpendicular to the c^* axis leading to space group *Pmma*. The $0kl$ and $1kl$ layer photographs of $CaPdIn_4$ indicated a *C*-centred lattice and the extinctions were compatible with space group *Cmcm*. All relevant crystallographic data and experimental details are listed in Table 1.

The atomic parameters of $YNiAl_4$[25] were taken for the structure refinement of $CaPdIn_4$; the starting atomic parameters for $CaRhIn_4$ and $CaIrIn_4$ were obtained from automatic interpretations of direct methods with SHELXS-97.[26] The structures were subsequently refined with anisotropic displacement parameters for all atoms with SHELXL-97.[27]

Final difference Fourier syntheses were flat and revealed no significant residual peaks. The results of the refinements are summarized in Table 1. Atomic coordinates and interatomic distances are listed in Tables 3 and 4. Further details of the crystal structure investigations can be obtained from the Fachinformationszentrum Karlsruhe, D-76344 Eggenstein-Leopoldshafen, Germany (fax: (+49) 7247-808-666; e-mail: crysdata@fiz-karlsruhe.de), on quoting the depository numbers CSD-410890 ($CaPdIn_4$), CSD-410891 ($CaRhIn_4$) and CSD-410892 ($CaIrIn_4$).

Crystal chemistry: The ternary compounds $CaTIn_4$ (T = Rh, Pd, Ir) are novel. They constitute the third structural type recognized so far in these ternary systems. Besides the equiatomic AlB_2-related compounds CaPdIn[28] and CaRhIn,[9] T-filled $CaIn_2$ compounds $CaTIn_2$[8, 9] have been found. The $CaTIn_4$ series seem to be the most indium-rich compounds among these calcium–transition metal–indium systems. Two structural types, $YNiAl_4$[25] and $LaCoAl_4$,[29] have been identified for the 1:1:4 composition. All the cobalt- and the new rhodium- and iridium-containing 1:1:4 compounds crystallize with the latter structure, whereas ternary nickel and palladium compounds adopt the $YNiAl_4$-type structure. With copper only $EuCuIn_4$[1, 14] is known. This clear separation into two groups (Co, Rh, Ir; and Ni, Pd, Cu) may be indicative of size restrictions imposed by the transition metal, and/or the electron count may determine which structural type is more favourable. It is unlikely that the structural change depends solely on the size of the electropositive element occupying the yttrium or lanthanum position, because the switch in structure type is also observed for $YbRhIn_4$[30] and $YbPdIn_4$.[31] Two different structure types are also observed for $CaRhIn_2$[9] and $CaPdIn_2$.[8]

Table 3. Atomic coordinates and isotropic displacement parameters [pm^2] for $CaPdIn_4$, $CaRhIn_4$ and $CaIrIn_4$. U_{eq} is defined as one third of the trace of the orthogonalized U_{ij} tensor.

Atom	Wyckoff site	*x*	*y*	*z*	U_{eq}
$CaRhIn_4$ (space group *Pmma*)					
Ca	2*e*	1/4	0	0.4002(3)	144(4)
Rh	2*e*	1/4	0	0.80781(9)	72(2)
In1	2*a*	0	0	0	126(2)
In2	2*f*	1/4	1/2	0.06525(8)	97(2)
In3	4*j*	0.06444(5)	1/2	0.68673(6)	103(2)
$CaPdIn_4$ (space group *Cmcm*)					
Ca	4*c*	0	0.12770(9)	1/4	139(3)
Pd	4*c*	0	0.77253(3)	1/4	104(1)
In1	8*f*	0	0.31698(2)	0.05040(5)	105(1)
In2	4*c*	0	0.93358(3)	1/4	158(1)
In3	4*b*	0	1/2	0	183(1)
$CaIrIn_4$ (space group *Pmma*)					
Ca	2*e*	1/4	0	0.4008(6)	143(9)
Ir	2*e*	1/4	0	0.8068(1)	64(2)
In1	2*a*	0	0	0	127(4)
In2	2*f*	1/4	1/2	0.0662(2)	92(3)
In3	4*j*	0.0651(1)	1/2	0.6854(1)	96(3)

The geometrical relationship between the structure types Re_3B,[32] $MgCuAl_2$[33] and $YNiAl_4$[25] has been discussed in detail elsewhere.[13, 25] Geometrically $CaPdIn_4$ can be considered to be an indium-filled $CaPdIn_2$ ($MgCuAl_2$ type[33]), which itself may be seen as a palladium-filled $CaIn_2$.[12] The indium atoms in $CaPdIn_2$ form a three-dimensionally infinite network of puckered indium layers which are topologically equivalent to hexagonal diamond[11] (lonsdaleite). By inserting zig-zag chains of indium atoms one obtains the $CaPdIn_4$ structure (Figure 2). Consequently, $CaPdIn_4$ contains puckered eight-membered indium rings and distorted *bcc*-like indium cubes.

The structure of $CaRhIn_4$ ($CaIrIn_4$) may be derived from binary $RhIn_3$[17] ($FeGa_3$ type, Figure 3). $RhIn_3$ is built up from *bcc*-like indium cubes and rhodium-filled trigonal prisms formed by the square faces of the cubes. Cutting $RhIn_3$ into slices and inserting calcium atoms leads formally to $CaRhIn_4$. The cubes and the trigonal prisms are retained in the form of zig-zag ribbons, separated by calcium layers. The calcium atoms are situated in distorted pentagonal prisms formed by

Table 4. Interatomic distances [pm] in the structures of $CaRhIn_4$, $CaPdIn_4$ and $CaIrIn_4$ calculated with the lattice constants obtained from Guinier powder data. All distances of the first coordination sphere are listed.

	$CaRhIn_4$				$CaPdIn_4$				$CaIrIn_4$			
Ca:	1	Rh	303.8(2)	Ca:	1	In2	323.2(3)	Ca:	1	Ir	303.0(4)
	2	In2	327.1(2)		2	Pd	328.7(2)		2	In2	327.6(3)
	4	In3	340.9(1)		4	In1	331.2(2)		4	In3	340.5(3)
	4	In3	351.2(1)		2	In1	349.3(2)		4	In3	352.4(1)
	2	In1	368.7(2)		4	In3	361.5(2)		2	In1	369.8(4)
					2	In2	390.7(3)				
Rh:	2	In1	259.9(1)					Ir:	2	In1	260.9(1)
	4	In3	280.7(1)	Pd:	1	In2	268.1(2)		4	In3	280.1(1)
	2	In2	285.5(1)		2	In1	271.2(1)		2	In2	287.2(1)
	1	Ca	303.8(2)		4	In1	279.3(1)		1	Ca	303.0(4)
					2	Ca	328.7(2)				
In1:	2	Rh	259.9(1)					In1:	2	Ir	260.9(1)
	4	In2	306.8(1)	In1:	1	Pd	271.2(1)		4	In2	307.7(1)
	4	In3	319.9(1)		2	Pd	279.3(1)		4	In3	321.4(1)
	2	Ca	368.7(2)		1	In1	301.1(2)		2	Ca	369.8(4)
					1	In3	307.1(2)				
In2:	2	Rh	285.5(1)		2	In1	324.7(2)	In2:	2	Ir	287.2(1)
	4	In1	306.8(1)		2	Ca1	331.2(2)		4	In1	307.7(1)
	2	In3	324.8(1)		2	In2	332.0(1)		2	In3	326.5(2)
	2	Ca	327.1(2)		1	Ca	349.3(2)		2	Ca	327.6(3)
	2	In3	329.5(1)						2	In3	330.8(1)
				In2:	1	Pd	268.1(2)				
In3:	2	Rh	280.7(1)		4	In3	312.5(1)	In3:	2	Ir	281.1(1)
	1	In3	299.9(1)		1	Ca	323.2(3)		1	In3	299.1(2)
	2	In1	319.9(1)		4	In1	332.0(1)		2	In1	321.4(1)
	1	In3	322.0(1)		2	Ca	390.7(3)		1	In3	321.5(2)
	1	In2	324.8(1)						1	In2	326.5(1)
	1	In2	329.5(1)	In3:	2	In1	307.1(2)		1	In2	330.8(1)
	2	Ca	340.9(1)		4	In2	312.5(1)		2	Ca	340.5(3)
	2	Ca	351.2(1)		4	Ca	361.5(2)		2	Ca	352.4(1)
					2	In3	377.2(3)				

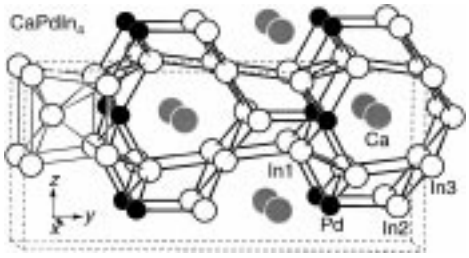

Figure 2. Crystal structure of $CaPdIn_4$ viewed along approximately the x axis. The calcium, palladium and indium atoms are represented by grey, black and open circles, respectively. The three-dimensional $[PdIn_4]$ polyanion is emphasized. A *bcc*-like cube of indium atoms is outlined in the upper left-hand corner of the unit cell.

indium atoms. The indium cubes in ternary $CaRhIn_4$ are greatly contracted in comparison with binary $RhIn_3$.

The near-neighbour environments in $CaPdIn_4$ and $CaRhIn_4$ show differences mainly in the coordination number (CN) of the calcium atoms. Calcium has CN 13 ($1 \times$ Rh and $12 \times$ In) in $CaRhIn_4$ and CN 15 ($2 \times$ Pd and $13 \times$ In) in $CaPdIn_4$. Palladium and rhodium have nine near neighbours each: $7 \times$ In and $2 \times$ Ca in $CaPdIn_4$ and $8 \times$ In and $1 \times$ Ca in $CaRhIn_4$. The indium atoms of the two ternary structure types all have very similar near-neighbour environments with CN 12 (Figure 4). In1 and In2 of $CaRhIn_4$ and In2 and In3 of $CaPdIn_4$ are situated in distorted cube-like indium polyhedra which are augmented by four additional neighbours. In3 ($CaRhIn_4$) and In1 ($CaPdIn_4$) have similar environments too, but these do not resemble cubes.

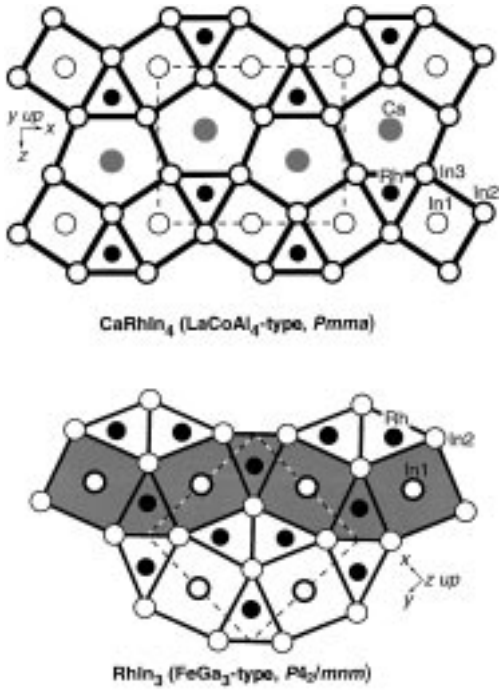

Figure 3. Projections of the crystal structures of $CaRhIn_4$ (top) and binary $RhIn_3$ (bottom). In $CaRhIn_4$ all atoms lie on mirror planes at $y = 0$ and $1/2$. Calcium, rhodium and indium atoms are represented by grey, black and open circles, respectively. The In2 and In3 atoms at $y = 1/2$, connected by thick lines, form three types of channels, trigonal, square and pentagonal, which are filled by rhodium, indium and calcium atoms respectively. In $RhIn_3$ a chain of alternating cubes and trigonal prisms is highlighted; this is observed in ternary $CaRhIn_4$ also.

0947-6539/00/0604-0604 $ 17.50+.50/0 *Chem. Eur. J.* **2000**, *6*, No. 4

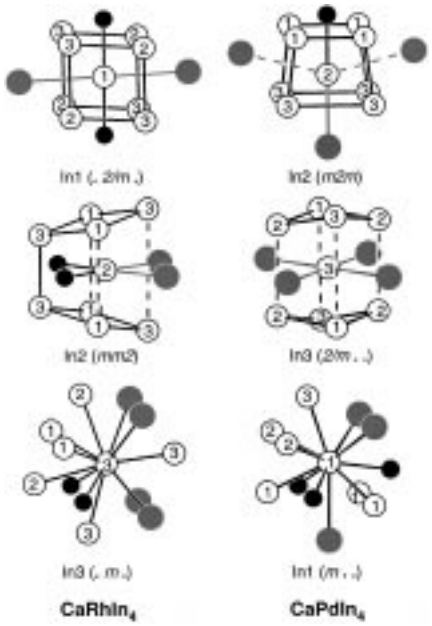

Figure 4. Near-neighbour environments of the three indium sites in the structures of $CaRhIn_4$ (left) and $CaPdIn_4$ (right). Site symmetries are given in parentheses. Numbers correspond to the atom designations. Broken grey lines indicate weak indium–calcium interactions, whereas broken black lines are only guides for the eye. The relationship with *cube*-like arrangements of the indium sites In1 and In2 in $CaRhIn_4$ and In2 and In3 in $CaPdIn_4$ is emphasized.

The shortest average bond lengths in $CaRhIn_4$ and $CaPdIn_4$ occur for Rh–In (277 pm) and Pd–In (275) contacts, respectively (Table 4). They are close to the sum of the metallic single-bond radii: 275 pm for Rh–In and 278 pm for Pd–In (data from Pauling[34]). The average In–In bond lengths of 316 pm ($CaRhIn_4$) and 324 pm ($CaPdIn_4$) are longer than the sum of the metallic single-bond radii (299 pm). The situation in $CaIrIn_4$ is quite similar to that in $CaRhIn_4$ and is not discussed here in greater detail.

The Ca–Rh(Ir) bond lengths, 304(303) pm, is only slightly longer than the sum of the metallic single-bond radii, 299(300) pm. However, in $CaPdIn_4$ the Ca–Pd contacts are somewhat greater (329 pm, compared with the sum of the metallic single-bond radii, 302 pm). The Ca–In contacts cover a wider range of distances: 327–369(328–370) pm in $CaRhIn_4$($CaIrIn_4$) and 323–391 pm in $CaPdIn_4$. However, each of the shortest Ca–In contacts matches well the sum of the metallic single-bond radii (323 pm).

To investigate further the variation of the bond lengths and for a more detailed electronic evaluation we carried out semi-empirical band structure calculations on all three compounds. The results are summarized in Table 5, but density of states (DOS) and semi-empirical crystal orbital overlap population (COOP) curves have been generated only for $CaRhIn_4$ and $CaPdIn_4$. The DOS curves for $CaRhIn_4$ and $CaPdIn_4$ are very similar (Figure 5). The rhodium(palladium) d states remain narrow and are centred near $-12(-9)$ eV, mixing with very broadened indium states, which cover the range from -15 eV up to and beyond the Fermi level. Calcium contributions are basically negligible below the Fermi level, suggesting the formulae $Ca^{2+}[RhIn_4]^{2-}$ and $Ca^{2+}[PdIn_4]^{2-}$. The expected

Table 5. Net charges (q) and overlap populations (OP) for $CaRhIn_4$, $CaPdIn_4$ and $CaIrIn_4$ as obtained from the extended Hückel calculations. T denotes the respective transition metal. Distances are given in pm.

	$CaRhIn_4$	$CaPdIn_4$	$CaIrIn_4$
q (Ca)	+1.60	+1.69	+1.76
q (T)	−1.28	−0.93	−1.93
q $(In)_{average}$	−0.08	−0.19	+0.04
q (In1)	+0.12	−0.12	+0.30
q (In2)	−0.03	−0.14	+0.05
q (In3)	−0.20	−0.38	−0.09
OP (Ca-T)	+0.096	±0.000	+0.113
OP (Ca-In)	+0.081	+0.085	+0.056
OP $(Ca\text{-}In)_{short}$	+0.160	+0.190	+0.139
	327	323	328
OP (T-In)	+0.199	+0.339	+0.327
OP $(In\text{-}In)_{average}$	+0.381	+0.330	+0.348
OP $(In\text{-}In)_{short}$	+0.672	+0.485	+0.680
	300	301–307	299
OP $(In\text{-}In)_{long}$	+0.310	+0.253	+0.267
	307–330	313–377	308–331

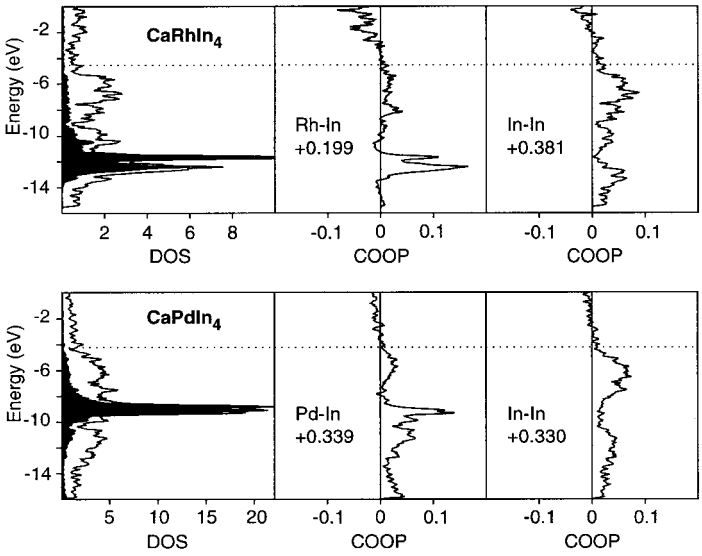

Figure 5. Total and projected DOS curves for $CaRhIn_4$ (top, left) and $CaPdIn_4$ (bottom, left). The rhodium or palladium contributions respectively are emphasized in black. The COOP curves for the Rh(Pd)–In and In–In interactions are shown (middle and right) with the integrated values of the overlap population.

d-band filling is evident for rhodium and palladium, and is even more pronounced for iridium, considering the net Mulliken charges (Table 4) of -1.28 (Rh), -0.93 (Pd) and -1.93 (Ir). The variation of the net charges approximately follows the absolute electronegativities according to Pearson[35] (rhodium 4.3 eV, palladium 4.45 eV and iridium 5.4 eV). Calcium, the least electronegative component, has high positive charges, whereas the charges of the three indium sites average close to zero for $CaRhIn_4$ and $CaIrIn_4$. For $CaPdIn_4$ the In3 site has no palladium neighbours and consequently it has a more negative charge, leading to a more negative average charge than the corresponding rhodium or iridium compound.

The COOP curves show the dominant presence of strongly bonding transition metal–indium and indium–indium interactions. For the latter the shorter contacts have higher overlap populations (OP) than the longer ones. Generally, only bonding interactions occur below the Fermi level and slightly

above. Ca–Rh, Ca–Pd, Ca–Ir and Ca–In bonding interactions surely play only a subordinate role.

One should bear in mind that the rhodium(iridium) compound has a lower electron count than the palladium compound. From the above results the electronic structures can safely be assumed to be optimized. Thus, by adopting different crystal structures, rhodium(iridium) and palladium each achieves a maximum filling of their d bands, while adequate In–In bonding is still present. Because of the higher electron count in $CaPdIn_4$, more electrons are available for In–In bonding. This is expressed by the occurrence of one indium site in $CaPdIn_4$ which has no palladium contacts. On the other hand the palladium atoms may have one fewer indium neighbour in their coordination sphere than the rhodium(iridium) atoms, because they have more electrons from the beginning.

The average In–In bond lengths are still longer in the ternary compounds $YCoIn_5$ and Y_2CoIn_8,[15] with only a slightly higher indium content (Figure 6). In–In bond lengths

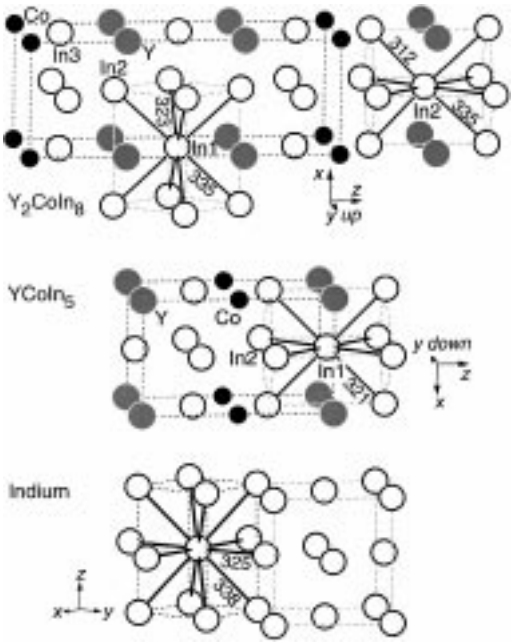

Figure 6. Distorted *bcc* indium cubes, emphasized by dotted lines, in the indium-rich compounds Y_2CoIn_8 (top) and $YCoIn_5$ (middle), compared with elemental indium (bottom). Relevant bond lengths [pm] are given. Atom designations correspond to those of Refs. [11] and [15]. In the case of indium the relationship of the tetragonal unit cell (broken lines) with the corresponding distorted face-centred pseudo cubic cell (dotted lines) is demonstrated.

are longer in elemental indium[11] as well. The greater In–In distances may be attributable to partial filling of antibonding In–In states. The two yttrium–cobalt–indium intermetallics can be regarded as derivatives of *fcc* arrangements. In indium itself, which has a tetragonally distorted *fcc* arrangement, the distortions are a consequence of the element having an electron deficiciency, which is compensated by formation of four short (325 pm) and eight longer (338 pm) interatomic bond lengths in contrast to the twelve equal distances an ideal *fcc* structure would require.[36] In $YCoIn_5$ and Y_2CoIn_8 some indium atoms have eight indium neighbours in the form of distorted cubes, which are augmented by four yttrium atoms. The central indium atom has no contacts with the cobalt atoms, presumably because the cobalt d bands are filled and there are electrons left for In–In bonding interactions. Nevertheless, the electron concentration is high and In–In bond lengths are longer.

Thus, $CaRhIn_4$($CaIrIn_4$) and $CaPdIn_4$ are in line with the known indium-rich compounds which may be expected to be more similar to elemental indium; at least, one should find fragments of elemental indium. The same holds true for borides with dominant boron networks or for polyphospides in which the elemental structural features of black phosporus become evident.[37] This contrasts with aluminides, in which a rich crystal chemistry is observed but without a tendency towards similarity to the elemental *fcc* aluminium structure.[38]

Acknowledgment

We thank Professor W. Jeitschko for his support of this work. Special thanks go to Dipl.-Ing. U. Ch. Rodewald for the intensity data collection and to Dr. W. Gerhartz (Degussa AG) for generous gifts of noble metals. This work was supported by the Deutsche Forschungsgemeinschaft and the Fonds der Chemischen Industrie.

[1] L. V. Sysa, Ya. M. Kalychak, *Crystallogr. Rep.* **1993**, *38*, 278.
[2] L. V. Sysa, Ya. M. Kalychak, *Inorg. Mater.* **1994**, *30*, 725.
[3] V. I. Zaremba, O. Ya. Zakharko, Ya. M. Kalychak, O. I. Bodak, *Dokl. Akad. Nauk Ukr. SSR*, *Ser. B* **1987**, *12*, 45.
[4] D. Kußmann, R.-D. Hoffmann, R. Pöttgen, *Z. Anorg. Allg. Chem.* **1998**, *624*, 1727.
[5] R.-D. Hoffmann, R. Pöttgen, *Z. Anorg. Allg. Chem.* **1999**, *625*, 994.
[6] R. Pöttgen, R.-D. Hoffmann, M. H. Möller, G. Kotzyba, B. Künnen, C. Rosenhahn, B. D. Mosel, *J. Solid State Chem.* **1999**, *145*, 174.
[7] R.-D. Hoffmann, R. Pöttgen, *Z. Kristallogr.* **1999**, *Suppl. 16*, 38.
[8] R.-D. Hoffmann, R. Pöttgen, G. A. Landrum, R. Dronskowski, B. Künnen, G. Kotzyba, *Z. Anorg. Allg. Chem.* **1999**, *625*, 789.
[9] R.-D. Hoffmann, R. Pöttgen, *Z. Anorg. Allg. Chem.* **2000**, in press.
[10] R.-D. Hoffmann, U. Ch. Rodewald, R. Pöttgen, *Z. Naturforsch. Teil B* **1999**, *54*, 38.
[11] J. Donohue, *The Structures of the Elements*, Wiley, New York, **1974**.
[12] A. Iandelli, *Z. Anorg. Allg. Chem.* **1964**, *330*, 221.
[13] R. Pöttgen, R. Müllmann, B. D. Mosel, H. Eckert, *J. Mater. Chem.* **1996**, *6*, 801.
[14] W. Schnelle, R. K. Kremer, R.-D. Hoffmann, R. Pöttgen, unpublished results.
[15] Ya. M. Kalychak, V. I. Zaremba, V. M. Baranyak, *Isv. Akad. Nauk SSSR Met.* **1989**, *1*, 209.
[16] R. Pöttgen, *J. Alloys Compd.* **1995**, *226*, 59.
[17] R. Pöttgen, R.-D. Hoffmann, G. Kotzyba, *Z. Anorg. Allg. Chem.* **1998**, *624*, 244.
[18] K. Yvon, W. Jeitschko, E. Parthé, *J. Appl. Crystallogr.* **1977**, *10*, 73.
[19] R. Hoffmann, *J. Chem. Phys.* **1963**, *39*, 1397.
[20] R. Hoffmann, *Solids and Surfaces: A Chemist's View of Bonding in Extended Structures*, VCH, Weinheim, **1988**.
[21] J. H. Ammeter, H.-B. Bürgi, J. C. Thibeault, R. Hoffmann, *J. Am. Chem. Soc.* **1978**, *100*, 3686.
[22] J. P. Desclaux, *At. Data Nucl. Data Tables* **1973**, *12*, 311.
[23] P. Pyykkö, L. L. Lohr Jr., *Inorg. Chem.* **1981**, *20*, 1950.
[24] G. A. Landrum, *Yaehmop—Yet Another Extended Hückel Molecular Orbital Package*, Version 2.0, **1997**; available on: http://overlap.chem.cornell.edu:8080/yaehmop.html
[25] R. M. Rykhal', O. S. Zarechnyuk, Ya. P. Yarmolyuk, *Sov. Phys. Crystallogr.* **1972**, *17*, 453.

0947-6539/00/0604-0606 $ 17.50+.50/0 *Chem. Eur. J.* **2000**, *6*, No. 4

[26] G. M. Sheldrick, *SHELXS-97, Program for the Determination of Crystal Structures*, University of Göttingen, **1997**.
[27] G. M. Sheldrick, *SHELXL-97, Program for Crystal Structure Refinement*, University of Göttingen, **1997**.
[28] S. Cirafici, A. Palenzona, F. Canepa, *J. Less-Common Met.* **1985**, *107*, 179.
[29] R. M. Rykhal', O. S. Zarechnjuk, Ja. P. Larmoljuk, *Dopov. Akad. Nauk Ukr. RSR*, *Ser. A* **1977**, *39*, 265.
[30] R.-D. Hoffmann, R. Pöttgen, unpublished results.
[31] R.-D. Hoffmann, V. I. Zaremba, R. Pöttgen, unpublished results.
[32] B. Aronsson, M. Bäckman, S. Rundqvist, *Acta Chem. Scand.* **1960**, *14*, 1001.
[33] H. Perlitz, A. Westgren, *Ark. Kemi*, *Miner. Geol.* **1943**, *16B*, 1.
[34] L. Pauling, *The Nature of the Chemical Bond and the Structure of Molecules and Crystals*, Cornell University Press, Ithaca, NY, **1960**.
[35] R. G. Pearson, *Inorg. Chem.* **1988**, *27*, 734.
[36] U. Häussermann, S. I. Simak, R. Ahuja, B. Johansson, S. Lidin, *Angew. Chem.* **1999**, *111*, 2155; *Angew. Chem. Int. Ed.* **1999**, *38*, 2017.
[37] H. G. von Schnering, W. Hönle, *Phosphides: Solid State Chemistry*, *Encyclopedia of Inorganic Chemistry* (Ed.: R. Bruce King), Wiley, London, **1994**.
[38] R. Nesper, *Angew. Chem.* **1991**, *103*, 805; *Angew. Chem.* **1991**, *30*, 789.

Received: July 19, 1999 [F1923]